

Study and circuit design of stochastic resonance system based on memristor chaos induction

Qi Liang(梁琦), Wen-Xin Yu(于文新), and Qiu-Mei Xiao(肖求美)

Citation: Chin. Phys. B, 2025, 34 (**4**): 040502. DOI: 10.1088/1674-1056/adb268
Journal homepage: http://cpb.iphy.ac.cn; http://iopscience.iop.org/cpb

What follows is a list of articles you may be interested in

Dynamics and synchronization of neural models with memristive membranes under energy coupling

Jingyue Wan(万婧玥), Fuqiang Wu(吴富强), Jun Ma(马军), and Wenshuai Wang(汪文帅)
Chin. Phys. B, 2024, 33 (**5**): 050504. DOI: 10.1088/1674-1056/ad1dcc

Fractional-order heterogeneous memristive Rulkov neuronal network and its medical image watermarking application

Dawei Ding(丁大为), Yan Niu(牛炎), Hongwei Zhang(张红伟), Zongli Yang(杨宗立), Jin Wang(王金), Wei Wang(王威), and Mouyuan Wang(王谋媛)
Chin. Phys. B, 2024, 33 (**5**): 050503. DOI: 10.1088/1674-1056/ad322b

Dynamics analysis and cryptographic implementation of a fractional-order memristive cellular neural network model

Xinwei Zhou(周新卫), Donghua Jiang(蒋东华), Jean De Dieu Nkapkop, Musheer Ahmad, Jules Tagne Fossi, Nestor Tsafack, and Jianhua Wu(吴建华)
Chin. Phys. B, 2024, 33 (**4**): 040506. DOI: 10.1088/1674-1056/ad03dd

Coexistence behavior of asymmetric attractors in hyperbolic-type memristive Hopfield neural network and its application in image encryption

Xiaoxia Li(李晓霞), Qianqian He(何倩倩), Tianyi Yu(余天意),Zhuang Cai(才壮), and Guizhi Xu(徐桂芝)
Chin. Phys. B, 2024, 33 (**3**): 030505. DOI: 10.1088/1674-1056/acf281

Multiple mixed state variable incremental integration for reconstructing extreme multistability in a novel memristive hyperchaotic jerk system with multiple cubic nonlinearity

Meng-Jiao Wang(王梦蛟) and Lingfang Gu(辜玲芳)
Chin. Phys. B, 2024, 33 (**2**): 020504. DOI: 10.1088/1674-1056/acddd0

Study and circuit design of stochastic resonance system based on memristor chaos induction

Qi Liang(梁琦), Wen-Xin Yu(于文新)†, and Qiu-Mei Xiao(肖求美)

School of Information and Electrical Engineering, Hunan University of Science and Technology, Xiangtan 411100, *China*

(Received 1 December 2024; revised manuscript received 14 January 2025; accepted manuscript online 5 February 2025)

Memristor chaotic research has become a hotspot in the academic world. However, there is little exploration combining memristor and stochastic resonance, and the correlation research between chaos and stochastic resonance is still in the preliminary stage. In this paper, we focus on the stochastic resonance induced by memristor chaos, which enhances the dynamics of chaotic systems through the introduction of memristor and induces memristor stochastic resonance under certain conditions. First, the memristor chaos model is constructed, and the memristor stochastic resonance model is constructed by adjusting the parameters of the memristor chaos model. Second, the combination of dynamic analysis and experimental verification is used to analyze the memristor stochastic resonance and to investigate the trend of the output signal of the system under different amplitudes of the input signal. Finally, the practicality and reliability of the constructed model are further verified through the design and testing of the analog circuit, which provides strong support for the practical application of the memristor chaos-induced stochastic resonance model.

Keywords: memristor, chaos, stochastic resonance, circuits

PACS: 05.40.–a, 05.45.–a, 05.20.Dd, 05.20.Gg

DOI: 10.1088/1674-1056/adb268 **CSTR:** 32038.14.CPB.adb268

1. Introduction

As a new type of non-volatile storage element, memristor has become a research hotspot due to its memory characteristics and computational capability. It can simulate the synaptic behavior of biological neurons and has good potential in constructing complex circuits, implementing neural networks and exploring nonlinear dynamics. Chaos and stochastic resonance, as two important branches of nonlinear dynamics, have great significance for understanding the behavioral patterns of complex systems and optimizing information processing.

A chaotic circuit system based on a memristor enriches the dynamic behavior of the original circuit and provides greater flexibility for logic circuits and neural network applications.[1–3] The study of Ullah Shamsher *et al.*[4] emphasizes the important role of memristor chaos in enhancing communication security and privacy protection, providing a new perspective on cryptographic applications in the digital age. Ramamoorthy Ramesh *et al.*[5] proposed and investigated the dynamical behavior of a new memristor chaotic Sprott B system, which provides a new perspective for understanding and controlling the multistable dynamics of complex memristor chaotic systems. Li Chuang *et al.*[6] analyzed the effect of the serial–parallel memristors through a mathematical model and demonstrated the coexistence of multiple attractors for a variety of initial conditions and the serial–parallel memristors. Shenghao Jia *et al.*[7] proposed a multi-volume super chaotic system based on memristor and successfully implemented its FPGA digital circuit implementation. Memristor chaotic system theory is rich in dynamics and has great potential for smart grid data encryption,[8] image encryption,[9] auditory and visual senses,[10] etc, which not only promotes the development of nonlinear dynamics, but also provides a new means for information security, neuromorphic computing and other fields.

Chaos is the unpredictable, stochastic-like motion exhibited by a deterministic dynamical system due to its sensitivity to initial values, and stochastic resonance is the nonlinear effect of noise enhancing a characteristic signal. The two are closely related in dynamics, but there is a dearth of exploration on the interaction between the two in the current research context. Stochastic resonance is widely used in weak signal enhancement.[11,12] Shangbin Jiao *et al.*[13] constructed a cascaded stochastic resonance system based on a Gaussian bistable model and introduced a feedback mechanism to address the single-system limitation. Xiangrong Wang *et al.*[14] proposed an asymmetrically decoupled unsaturated bistable stochastic resonance system to overcome the limitations of traditional systems in extracting weak signal features. Fan Dai *et al.*[15] proposed an adaptive detection method based on a bistable system for the low signal-to-noise ratio (SNR) problem in aeromagnetic anomaly detection. In addition, stochastic resonance has shown great potential in the field of mechanical fault diagnosis.[16,17] There are numerous studies on stochastic resonance based on Duffing and Langevin equations, but there are fewer studies on chaos-induced stochastic

†Corresponding author. E-mail: 13874894700@163.com

© 2025 Chinese Physical Society and IOP Publishing Ltd. All rights, including for text and data mining, AI training, and similar technologies, are reserved.

resonance. Zhou Zuanbo *et al.*[18] investigated stochastic resonance in fractional-order Lorenz-like systems, demonstrated the dynamical process from the point of view of equilibrium, and connected chaotic and stochastic resonance, which provided a new idea of the conversion between the two.

The above studies show that the applications of chaos and stochastic resonance in dynamical systems are multifaceted and theoretically important. However, in the existing academic research, relatively little has been done to explore the correlation between the two. In this paper, a stochastic resonance system based on memristor chaos induction is proposed. In Section 2, a memristor chaos model is constructed, and the memristor chaos is used to induce stochastic resonance. In addition, the intrinsic relationship between memristor chaos and stochastic resonance is studied. Meanwhile, the dynamics of the constructed memristor stochastic resonance model is analyzed in this section, and the processing effect of the system on noise-containing as well as noise-free signals at the critical value is explored. In Section 3, circuit simulation experiments are carried out to verify the performance of the memristor chaos and its induced stochastic resonance and to assess its feasibility in practical applications. In Section 4, the content of this paper is summarized.

2. Memristor chaos-induced stochastic resonance studies

In this section, the basic concept of the memristor and its mathematical model are first systematically introduced. Subsequently, it is incorporated into the Lü chaotic model, which enriches the dynamical behavior of the chaotic system and allows the system to exhibit more complex and variable nonlinear dynamic properties. The stochastic resonance phenomenon is further induced by the nonlinear properties of memristor chaos and the adjustment of the system parameters. The performance of the memristor stochastic resonance model is verified through the dynamic analysis of the model, the processing effect on the noisy and non-noisy signals, and the processing effect at the critical value.

2.1. Memristor model

In Ref. [19], Chua proposed a generalized memristor model as

$$\begin{aligned} i(t) &= G(w)v(t), \\ \frac{\mathrm{d}w}{\mathrm{d}t} &= g(w,v), \end{aligned}$$

where $i(t)$ and $v(t)$ represent the output current source and input voltage source of the generalized memristor and w is the flux variable of the generalized memristor. In this paper, let $G(w) = 0.2 - 0.6\tanh(w)$, $g(w,v) = 0.1v - w$, where $\tanh(\cdot)$ is a hyperbolic tangent function. Then, a new generalized memristor model can be expressed as

$$\begin{aligned} i(t) &= [0.2 - 0.6\tanh(w)]v(t), \\ \frac{\mathrm{d}w}{\mathrm{d}t} &= 0.1v - w. \end{aligned} \tag{1}$$

A periodic excitation signal $v = A\sin(2\pi ft)$ is applied to both ends of the memristor, where the amplitude of the signal is A, the frequency is defined as f and the time variable is t. To systematically investigate the voltametric (v–i) characteristics of the memristor under different amplitude and frequency excitations, the fixed amplitude A of the excitation signal is first set at 10, and the frequency f of the excitation signal is adjusted and the v–i characteristic curve is recorded, as shown in Fig. 1(a). It is observed that with the gradual increase in the excitation signal frequency f, the hysteresis loop area presented by the memristor shows a decreasing trend until it finally converges to a straight line. Then, frequency f was fixed at 0.6, the amplitude A was varied and the curve was recorded, as shown in Fig. 1(b). It is observed that as the excitation signal amplitude A increases, the hysteresis loop area of the memristor increases accordingly and all the recorded v–i characteristic curves pass through the origin of the coordinates. This confirms the sensitivity of the memristor to the amplitude as well as the frequency of the excitation signal and reveals its nonlinear mechanism, which fulfills the requirements for the characterization of nonlinear memory elements.

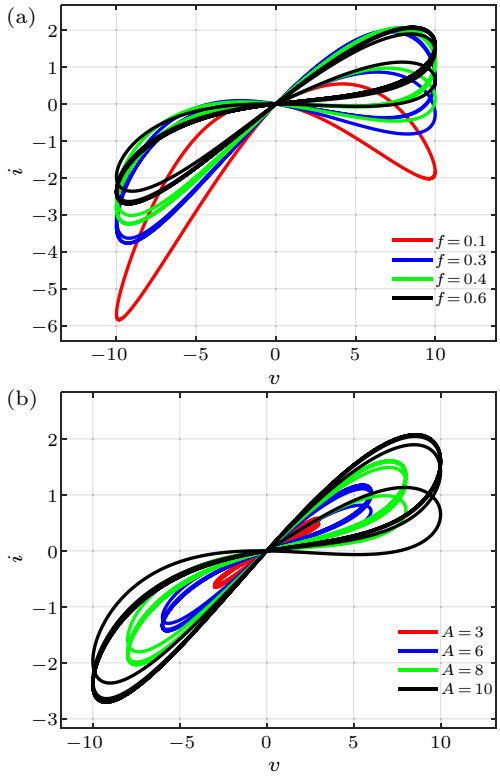


Fig. 1. Memristor model: (a) varying frequency f with fixed amplitude A of 10 and (b) varying amplitude A with fixed frequency f of 0.6.

2.2. Memristor chaos model

The memristor chaos established in Ref. [20] defines the magnetic flux flowing through the memristor as the fourth state variable w, while the state variable x is used as the voltage on both sides of the memristor and is introduced as a feedback into the Lü system. In addition, a memristor term is introduced in the state variable y to further strengthen the memristor property. By adjusting the system parameters, a fourth-order memristor chaotic system consisting of a memristor is constructed, and the mathematical model of this chaotic system is specifically formulated as

$$\begin{aligned} &\dot{x} = a(y-x), \quad \dot{y} = cy - xz + kxG(w), \\ &\dot{z} = xy - bz, \quad \dot{w} = ex - w. \end{aligned} \tag{2}$$

The dissipative nature of the system can be expressed by

$$\nabla V = \frac{\partial \dot{x}}{\partial x} + \frac{\partial \dot{y}}{\partial y} + \frac{\partial \dot{z}}{\partial z} + \frac{\partial \dot{w}}{\partial w} = -a + c - b - 1. \tag{3}$$

When the parameter $a = 36$, $b = 3$, $c = 20$, $e = 0.1$, $k = 1$, the above equation satisfies $-a + c - b - 1 < 0$, which is $\nabla V < 0$. This indicates that in the limit case where time tends to infinity, the dynamical trajectory of the system will always be confined to a specific, bounded region and exhibit dissipative properties, namely, the system is continuously emitting energy or information to the outside world while the volume of its own state space is gradually decreasing.

The state variables of the system are set at $\dot{x} = \dot{y} = \dot{z} = \dot{w} = 0$, from which we can determine the equilibrium point described by the system to be $(0, 0, 0, 0)$. To analyze the stability of this equilibrium point in depth, the Jacobi matrix of the system at the equilibrium point is calculated by

$$J_1 = \begin{bmatrix} -a & a & 0 & 0 \\ 0.2k & c & 0 & 0 \\ 0 & 0 & -b & 0 \\ e & 0 & 0 & -1 \end{bmatrix}. \tag{4}$$

We construct the characteristic polynomial $|\lambda E - J_1|$, where λE denotes the product of the eigenvalues λ and the unit matrix E. By solving this equation with a characteristic polynomial equal to zero as $|\lambda E - J_1| = 0$, we obtain the characteristic equation of the Jacobi matrix at the equilibrium point. The specific form of this characteristic equation is

$$(\lambda + 1)(\lambda + b)[\lambda^2 + (a - c)\lambda - a(c + 0.2k)] = 0. \tag{5}$$

Solving Eq. (5) yields $\lambda_{1,2} = \frac{-(a-c) \pm \sqrt{(a-c)^2 - 4a(a-c)(c-0.2k)}}{2}$, $\lambda_3 = -1$, $\lambda_4 = -b$. According to the Laws stability criterion, a sufficient condition for a system to be stable is that all the eigenvalues of its Jacobi matrix have negative real parts. If there are positive numbers in this eigenvalue, this is a direct indication that the system is unstable at the equilibrium point $(0, 0, 0, 0)$, representing the possibility of the system entering a chaotic or hyperchaotic state.

Here $G(w) = 0.2 - 0.6\tanh(w)$, we take $a = 36$, $b = 3$, $c = 20$, $e = 0.1$, $k = 1$ and the initial value $(0.2, 0.5, 0.3, 0.2)$, at which point the typical chaotic attractor exists in the system, whose phase diagram is shown in the circuit analysis in

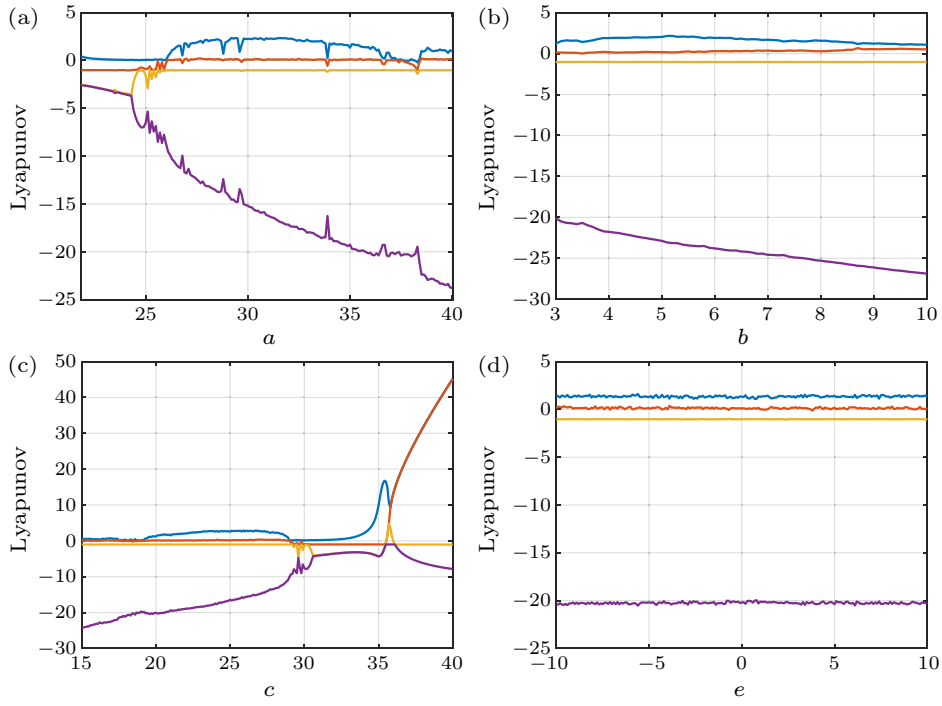


Fig. 2. Lyapunov exponential spectrum under different parameter conditions: (a) $a \in (20, 40)$, $b = 3$, $c = 20$, $e = 0.1$, $k = 1$; (b) $b \in (3, 10)$, $a = 36$, $c = 20$, $e = 0.1$, $k = 1$; (c) $c \in (15, 40)$, $a = 36$, $b = 3$, $e = 0.1$, $k = 1$; (d) $e \in (-10, 10)$, $a = 36$, $b = 3$, $c = 20$, $k = 1$.

Subsection 3.1. To observe and analyze the evolution of the trajectory of the chaotic dynamics of the system, this paper employs Lyapunov exponents of different variables as an analytical tool to portray the chaotic dynamic behavior of the system. Specifically, the value of parameter a, b, c, e was adjusted separately while keeping the other parameters constant, which in turn calculated and plotted the Lyapunov exponential diagram of the system under these parameter variations, as shown in Fig. 2. When the value of the maximum Lyapunov exponent is greater than 0 and the sum of the Lyapunov exponents is less than 0, the system is in a chaotic state.

2.3. Memristor stochastic resonance model

Variations in the response characteristics of the system are explored by making parameter adjustments based on the chaotic model described in Eq. (2). Meanwhile, to investigate the response mechanism of the system to external excitation, an input signal $S(t)$ is introduced in the y-dimension and the system equations evolve into the form

$$\begin{aligned} &\dot{x} = a(y-x), \quad \dot{y} = cy - xz + kxG(w) + S(t), \\ &\dot{z} = xy - bz, \quad \dot{w} = ex - w, \end{aligned} \tag{6}$$

where $G(w) = 0.2 - 0.6\tanh(w)$. Within the framework of this new system, it is further analyzed in terms of dynamics.

2.3.1. Equilibrium analysis

For the stochastic resonant system shown in Eq. (6), when the system is at equilibrium, there is

$$\begin{aligned} &a(y-x) = 0, \quad cy - xz + kx[0.2 - 0.6\tanh(w)] + S(t) = 0, \\ &xy - bz = 0, \quad ex - w = 0. \end{aligned} \tag{7}$$

In addition, the equation for the relationship between the state variables can be obtained as

$$x = y, \quad z = \frac{y^2}{b}, \quad w = ey. \tag{8}$$

Namely, the state variables x, z, w can all be represented by functions containing only the state variable y. It can also be said that state variables x, z, w can be seen as the output of further processing of state variable y.

Substituting Eq. (8) into $\dot{y} = cy - xz + kx[0.2 - 0.6\tanh(w)] + S(t) = 0$ yields the equation for the equilibrium point of the system

$$\dot{y} = cy - \frac{1}{b}y^3 + ky[0.2 - 0.6\tanh(ey)] + S(t) = 0. \tag{9}$$

Let $H(y) = \frac{1}{b}y^3 - (c + 0.2k)y + 0.6ky\tanh(ey)$, then $-H(y) + S(t) = 0$. The intersection of the system equilibrium curve $H(y)$ and $S(t)$ is the equilibrium point of the system, as shown in Eq. (6). The equilibrium point of the stochastic resonance system and the schematic diagram of the y-dimensional input-output are shown in Fig. 3, where the red line is $H(y)$ and the blue line is $S(t)$. $S(t)$ is a bounded weak signal, namely, for any t in the domain of definition, there is $S(t) = \mu$, $\mu \in R$, which is taken to means that there is and can be only one solution to $H(y) = S(t)$, which is the intersection of the two lines, as shown by the black dot in Fig. 3.

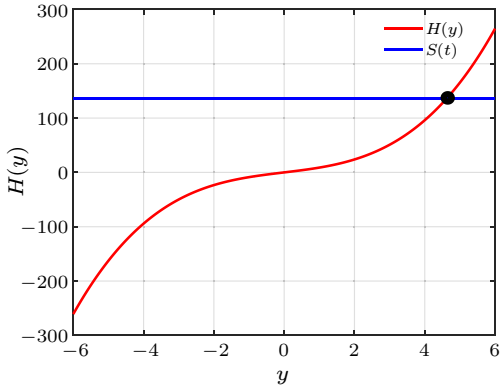


Fig. 3. Schematic diagram of system balance curve $H(y)$ and input signal $S(t)$.

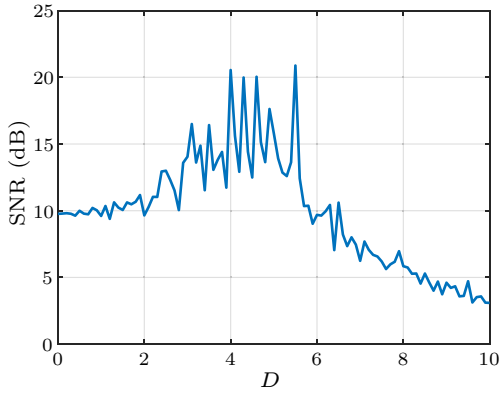


Fig. 4. Variation of output SNR with noise amplitude D.

To deeply analyze the dynamic relationship between the output SNR and the noise intensity D, the characteristic curve of the output SNR varying with the noise intensity is obtained using the numerical simulation method, and the result is visualized in Fig. 4. Observing the curve, the existence of a peak can be clearly seen, and this characteristic peak is a typical manifestation of the stochastic resonance phenomenon where the parameters take the values $a = 8$, $b = 3$, $c = -1$, $e = 0.1$, $k = 1$, $S(t) = m(t) + n(t)$. Here $n(t) = D\varepsilon(t)$, $\varepsilon(t)$ is white noise signals with mean 0 and variance 1, D is the noise amplitude; and $m(t) = A\sin(2\pi ft)$ with $A = 1$, $f = 0.05$ is the feature signal.

From Fig. 3, the system equilibrium curve $H(y)$ and the input signal $S(t)$ have only one intersection point, namely, the system will only have one equilibrium point at the same time. With the change of input, the position of the equilibrium point will be changed. Thus, the value of the y-dimensional out-

put of the system will be changed, and the rest of the three-dimensional output of the system will be changed by Eq. (8). The potential function is $G(y) = \int H(y)\mathrm{d}y$. We then obtain $G(y) = \int [\frac{1}{b}y^3 - (c+0.2k)y - 0.6ky\tanh(ey)]\mathrm{d}y$, set the parameters $a = 8$, $k = 1$, $c = -1$, change the values of b, e, and its potential function $G(y)$ image is shown in Fig. 5. This system is a slightly asymmetric monostable stochastic resonance system. The system has a stable solution and a potential well, no threshold and jump, no potential barriers, and the signal can obtain energy from the noise, along the edge of the potential well when the signal's energy increases at the same time as the energy of the noise decays.

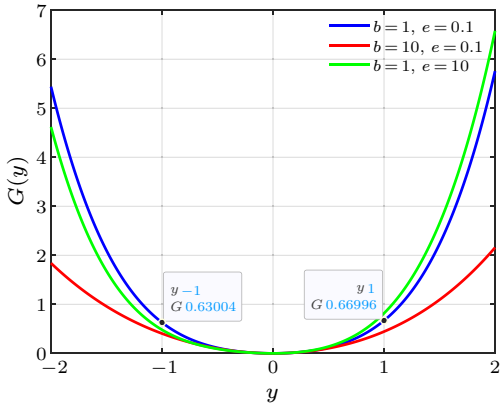


Fig. 5. Stochastic resonance system potential function $G(y)$.

The Jacobi matrix J of Eq. (6) is given by

$$J = \begin{bmatrix} -a & a & 0 & 0 \\ -z + k[0.2 - 0.6\tanh(w)] & c & -x & -0.6kx\{1 - [\tanh(w)]^2\} \\ y & x & -b & 0 \\ 0.1 & 0 & 0 & -1 \end{bmatrix}. \tag{10}$$

Substituting Eq. (8) into Eq. (10) gives

$$J = \begin{bmatrix} -a & a & 0 & 0 \\ -\frac{y^2}{b} + k[0.2 - 0.6\tanh(ey)] & c & -y & -0.6ky\{1 - [\tanh(ey)]^2\} \\ y & y & -b & 0 \\ 0.1 & 0 & 0 & -1 \end{bmatrix}. \tag{11}$$

Let $|J - rE| = 0$, where E is the unit matrix. Set the parameters $a = 8$, $b = 3$, $e = 0.1$, $c = -1$, $k = 1$ by solving the system Jacobian matrix corresponding to the eigenvalues r_1, r_2, r_3, r_4. The eigenvalue with y is shown in Fig. 6, and from the figure it can be seen that when $y \in R$, the eigenvalues are all less than 0, which demonstrates that the system's equilibrium is a stable equilibrium point.

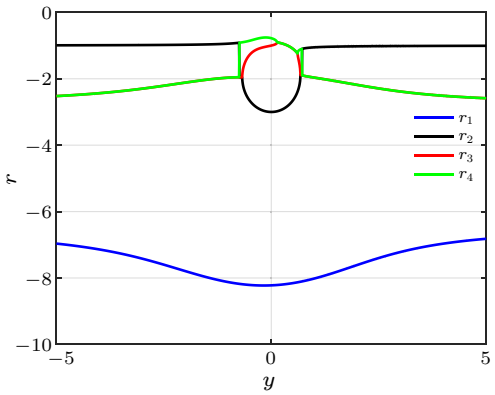


Fig. 6. Eigenvalues r of the stochastic resonance system.

2.3.2. Gain analysis

From Eq. (6), when the system is in equilibrium, $S(t) = \frac{1}{b}y^3 - (c+0.2k)y + 0.6ky\tanh(ey)$, so that y is the output dimension of the system. At the same time, the gain Q of the system is the ratio of the output y to the input $S(t)$. This gain value reflects the degree of amplification or reduction of the input signal of the system, which is an important indicator for assessing the performance of the system, and the specific expression is

$$Q = \frac{y}{S(t)} = \frac{y}{\frac{1}{b}y^3 - (c+0.2k)y + 0.6ky\tanh(ey)} = \frac{1}{\frac{1}{b}y^2 - (c+0.2k) + 0.6k\tanh(ey)}. \tag{12}$$

After substituting the parameters $a = 8$, $b = 3$, $c = -1$, $e = 0.1$, $k = 1$, $Q = \frac{3}{y^2+2.4+1.8\tanh(0.1y)}$, and a plot of the system gain versus y can be drawn, as shown in Fig. 7(a), so that the gain Q of the system will be greater than 1 when $y \in (-0.88, 0.73)$ is satisfied. It is also clear from Eq. (9) that the input signal $S(t)$ can be expressed as a function of only the variable y, and the relationship is visually demonstrated in Fig. 7(b). Specifically, when the input signal $S(t)$ satisfies $S(t) \in (-0.884813, 0.74559)$ and $y \in (-0.88, 0.73)$, namely, the gain Q of the system will be greater than 1, which means that the system has amplification of the input vibrational periodic signal. Therefore, at the same time, the amplitude change of the system output y is significantly amplified compared to the amplitude change of the input signal $S(t)$ so that the output release phenomenon occurs. Similarly, when the input signal

satisfies $S(t) \in (-\infty, -0.884813) \cup (0.74559, +\infty)$, the gain Q of the system will be less than 1. At the same time, the system will inhibit the change of the input oscillatory cycle signal, which means that the amplitude change of the output y of the system will be significantly reduced compared with the amplitude change of the input signal $S(t)$, and the output inhibition phenomenon occurs. The above analyses show that there are differences in the processing capability of the system for different input signals.

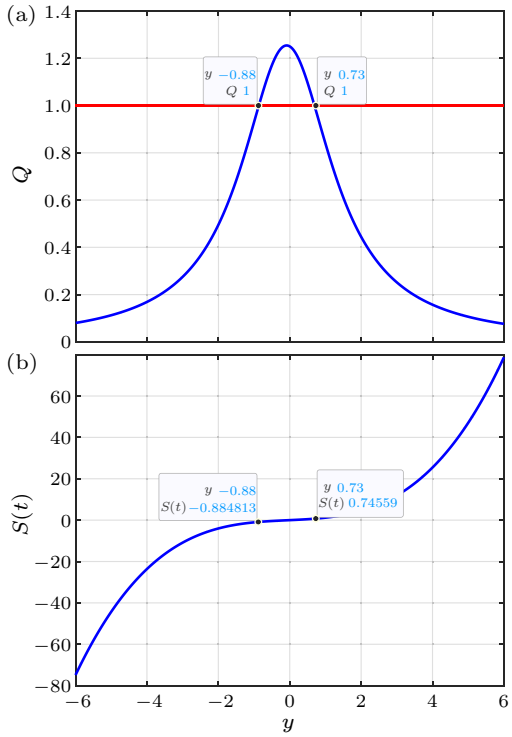


Fig. 7. Gain Q and input signal $S(t)$ versus system output y-dimensionally at specific parameters: (a) y–Q; (b) y–$S(t)$.

2.3.3. Simulation verification

Adjusting parameters $a = 8$, $b = 3$, $c = -1$, $e = 0.1$, $k = 1$ and setting the input signal as $S(t) = m(t)$, where $m(t) = A\sin(2\pi ft) = 1$ with $f = 0.05$ is used as the characteristic signal, the phase diagram of the system presents a periodic state under this condition, as shown in Fig. 8.

Under the above conditions, the output signal is shown in Fig. 9(a), which can be observed to scale the input signal to some extent. In particular, $z = y^2/b$ is obtained from Eq. (8) to ensure that the resulting sequence is all non-negative in the z dimension. Subsequently, changes in the stochastic resonance output were observed by varying the amplitude $A = 0.2$ of the feature signal. Under the adjusted conditions, the sequence diagram for each dimension is shown in Fig. 9(b), where the x and y dimensions amplify the input signal. After further adjusting the feature signal amplitude $A = 0.74559$, the sequence diagram for each dimension of the stochastic resonance output is shown in Fig. 9(c), at which time the input signals in the x and y dimensions are largely recovered. The above simulation results are consistent with the theoretical expectations and verify the effectiveness and accuracy of the experimental method. Given that the simulation is performed under ideal noise-free conditions, the output signal waveforms as illustrated in Figs. 9(a)–9(c) show a high degree of similarity between the output results in the x and y-dimensions.

Let the noise amplitude $D = 2$. Figure 10(a) shows the input signal $S(t)$ and the feature signal $m(t)$. The SNR of $S(t)$ is -8.8946 dB. It can be observed that the noise completely masks the feature signal at this time. Figure 10(b) shows the input signals x, y, z, w after random resonance, in which the y-dimensional output signal has an SNR of 14.1985 dB. Figure 10(c) shows the low-pass-filtered output signal Y, which has an SNR of 7.1493 dB. Although the results in the z and w dimensions are slightly unsatisfactory, the x and y dimensions have been more successful in restoring the main features of the original signal, with some fluctuation in the details only. In addition, it can be clearly observed that stochastic resonance is better at denoising effect.

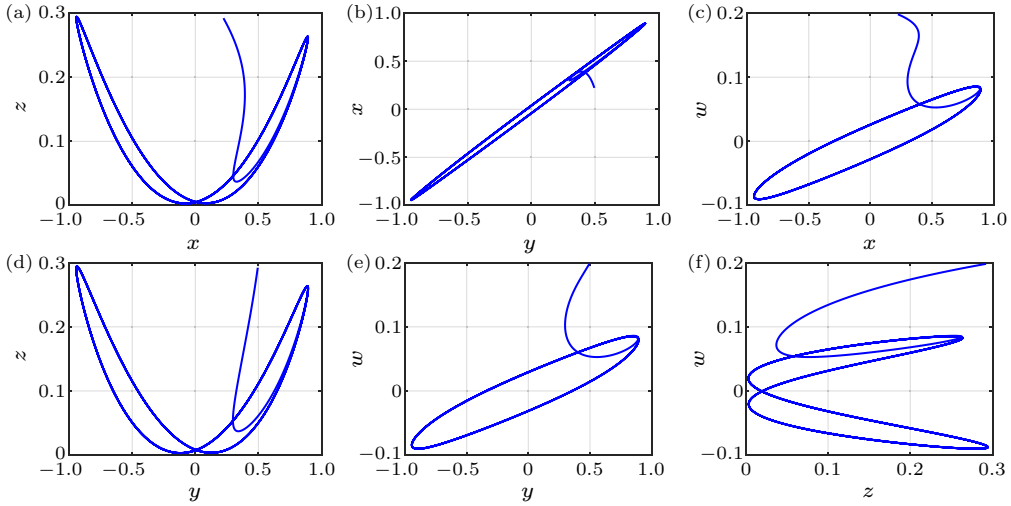


Fig. 8. Phase diagram of the stochastic resonant system when the input signal does not contain noise: (a) x–z; (b) y–x; (c) x–w; (d) y–z; (e) y–w; (f) z–w.

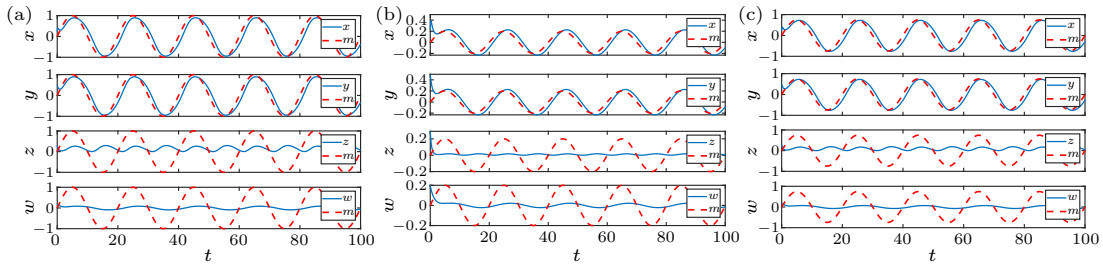


Fig. 9. Output waveforms of stochastic resonance system for input signals of different amplitudes in the absence of noise: (a) $A = 1$; (b) $A = 0.2$; (c) $A = 0.74559$.

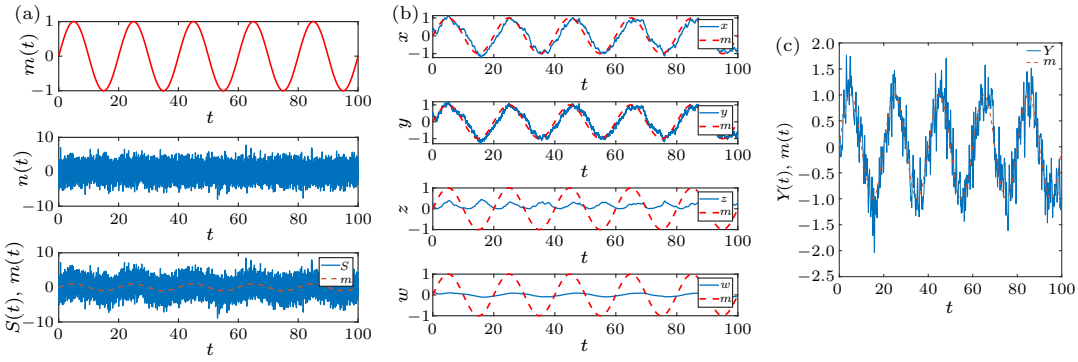


Fig. 10. Input and output waveforms of the stochastic resonance system when the input signal contains noise: (a) stochastic resonance input signal $S(t)$; (b) stochastic resonance output signals x, y, z, w; (c) low-pass filtered output signal Y.

3. Circuit experiments

To further validate the performance of the models of the memristor within the framework of chaotic dynamic behavior and the stochastic resonance theory based on it, as well as to assess the feasibility and practicability of these models in the design of electronic systems and real-world application scenarios, a series of circuit building and validation work is carried out in this section.

3.1. Memristor chaotic circuit design

The Multisim simulation platform is used to design and simulate the circuit of the hyperchaotic system, and the overall memristor chaotic circuit layout is shown in Fig. 11. In this design, the equivalent circuit module of the $\tanh(\cdot)$ function in the memristor is constructed using an operational amplifier together with a transistor as the w dimension in the circuit. A transistor is combined with resistive elements to form a stable constant current source. Furthermore, the circuit design employs the integration of an operational amplifier with a capacitor to implement the function of an inverse integrator; an inverter circuit is also constructed by combining the resistive components. To handle the nonlinear terms in the circuit, a multiplier component is introduced. The mathematical equations of the chaotic system are transformed into the corresponding circuit equations according to Kirchhoff's voltage law in the form

$$\begin{aligned}
\dot{v_x} &= -\frac{v_x}{R_7C_3} - \frac{-v_y}{R_8C_3},\\
\dot{v_y} &= -\frac{-v_y}{R_1C_1} - \frac{v_x\tanh(v_w)}{R_2C_1} - \frac{v_xv_z}{R_3C_1} - \frac{v_x}{R_4C_1},\\
\dot{v_z} &= -\frac{-v_xv_y}{R_9C_2} - \frac{v_z}{R_{10}C_2},\\
\dot{v_w} &= -\frac{-v_x}{R_{13}C_4} - \frac{v_w}{R_{14}C_4}.
\end{aligned} \tag{13}$$

The voltage across the components is at ± 18 V DC level to ensure that they operate within a safe supply voltage range. However, when the state variable in Eq. (13) is used as a voltage, it will exceed the supply voltage range of the components in the circuit, so the state variable of the system is compressed proportionally to make $x = 10v_x$, $y = 10v_y$, $z = 10v_z$. Since the state variable w as a voltage can satisfy the supply voltage range of the components, $w = v_w$, where the voltage applied to the integrating capacitor is v_x, v_y, v_z, v_w. The multiplier is chosen to be the AD633 multiplier with a multiplication factor of 0.1, and a time scale transformation of the transformation factor $\tau_0 = 100$. The final standardized equation is obtained as follows:

$$\begin{aligned}
\dot{v_x} &= -3600v_x + 3600v_y,\\
\dot{v_y} &= 2000v_y - 600v_x\tanh(v_w) - 10000v_xv_z + 20v_x,\\
\dot{v_z} &= 10000v_xv_y - 300v_z,\\
\dot{v_w} &= 100v_x - 100v_w.
\end{aligned} \tag{14}$$

$C_3 = 100$ nF, $C_1 = C_2 = C_4 = 1$ μF, $R_7 = R_8 = 2.8$ kΩ, $R_{13} = R_{14} = 10$ kΩ, $R_1 = 500$ Ω, $R_2 = 1.66$ kΩ, $R_3 = 100$ Ω, $R_4 = 50$ kΩ, $R_9 = 100$ Ω, $R_{10} = 3.3$ kΩ are calculated from Eqs. (13) and (14). Its specific circuit diagram is illustrated in Fig. 11, while the simulation result of the phase diagram is presented in Fig. 12. This result is consistent with the numerical simulation result, demonstrating evident chaotic characteristics.

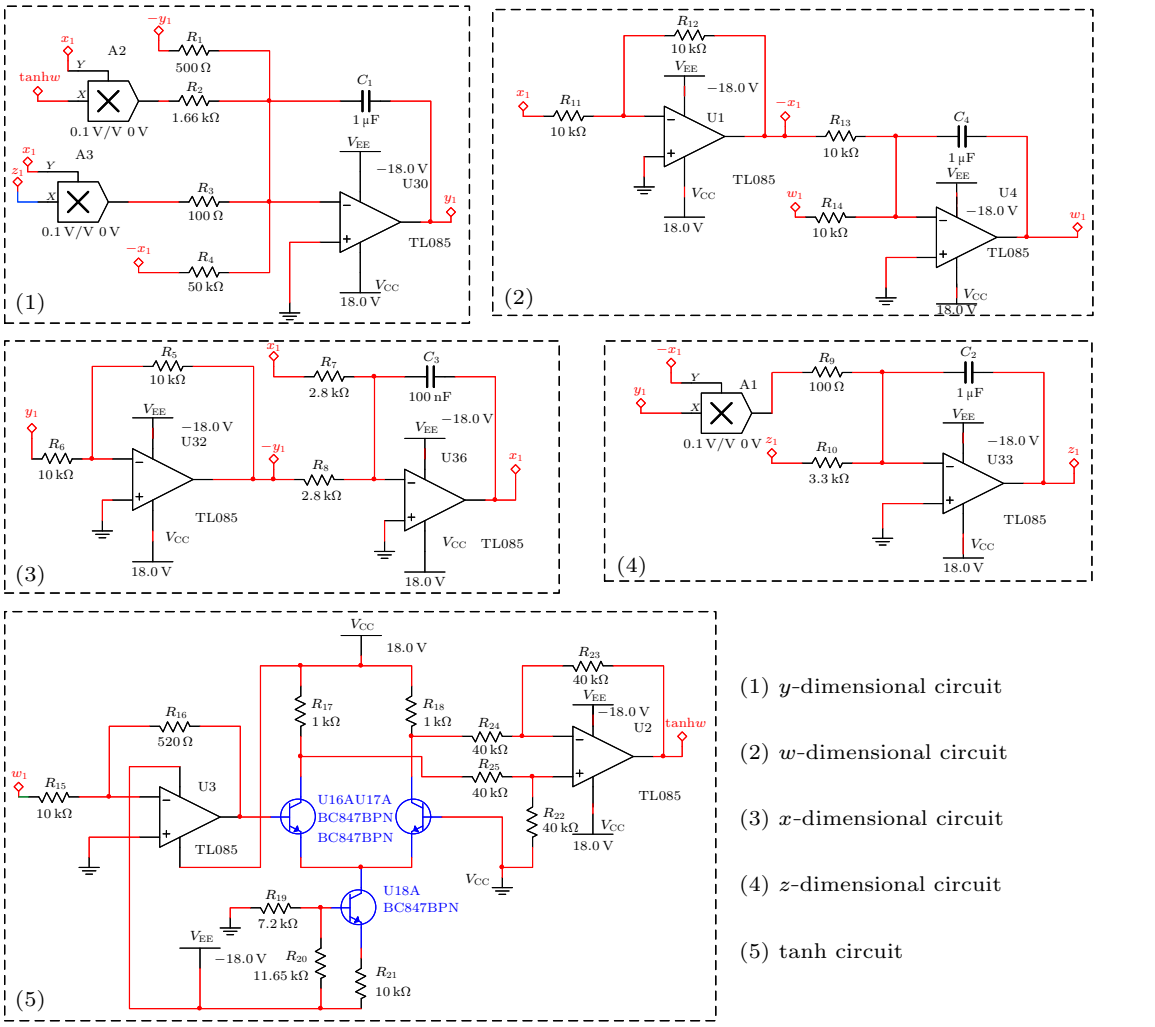


Fig. 11. Memristor chaotic circuit simulation implementation.

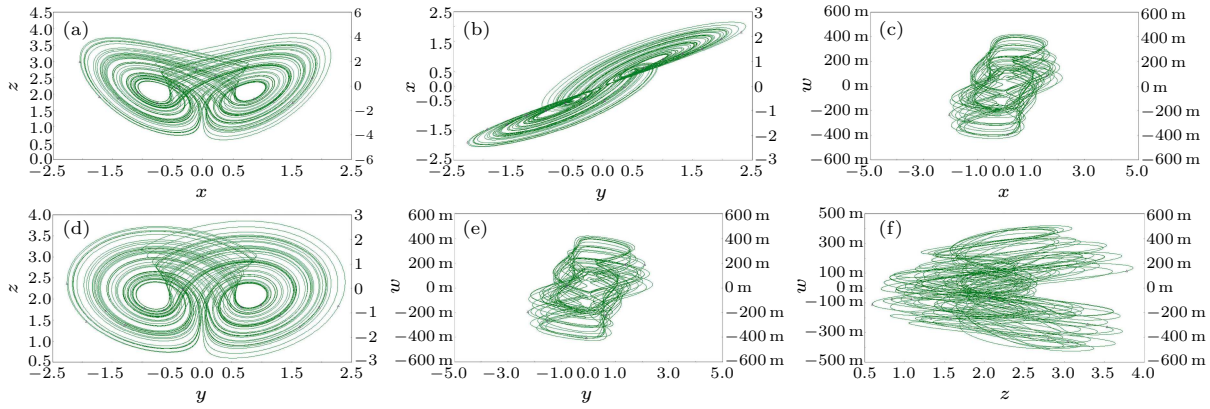


Fig. 12. Attractor phase diagram for memristor chaotic circuit simulation: (a) x–z; (b) y–x; (c) x–w; (d) y–z; (e) y–w; (f) z–w.

3.2. Memristor stochastic resonance circuit design

Similarly, the memristor stochastic resonance equation is expressed as the corresponding circuit equation

$$\dot{v_x} = -\frac{v_x}{R_7C_3} - \frac{-v_y}{R_8C_3},$$
$$\dot{v_y} = -\frac{-v_y}{R_1C_1} - \frac{v_x\tanh(v_w)}{R_2C_1} - \frac{v_xv_z}{R_3C_1} - \frac{v_x}{R_4C_1} - \left(\frac{-S(t)}{R_{28}C_1}\right),$$
$$\dot{v_z} = -\frac{-v_xv_y}{R_9C_2} - \frac{v_z}{R_{10}C_2},$$
$$\dot{v_w} = -\frac{-v_x}{R_{13}C_4} - \frac{v_w}{R_{14}C_4}. \tag{15}$$

The voltage across the terminals of the components is ±18 V. The physical meaning of the state variables defined in Eq. (15) corresponds to the value of the voltage applied across the components in the circuit, which is within the range of the power supply voltage set above. Therefore, there is no need to compress the state variables of the system here. For signal processing and computation, the AD633 multiplier was selected with

a multiplication factor set at 0.1 to meet specific circuit design requirements. In addition, to convert the original equations into a normalized form that is easier to analyze and process, a time scale transformation is performed, which introduces the transformation factor $\tau_0 = 100$. Through this transformation process, we finally obtain the normalized equations

$$\begin{aligned}
\dot{v_x} &= -800v_x + 800v_y,\\
\dot{v_y} &= -100v_y - 600v_x\tanh(v_w) - 1000v_xv_z + 20v_x + S(t),\\
\dot{v_z} &= 1000v_xv_y - 300v_z,\\
\dot{v_w} &= 10v_x - 100v_w.
\end{aligned} \tag{16}$$

$C_3 = 100$ nF, $C_1 = C_2 = C_4 = 1$ μF, $R_7 = R_8 = 12.5$ kΩ, $R_{13} = 100$ kΩ, $R_1 = R_{14} = R_{28} = 10$ kΩ, $R_2 = 1.66$ kΩ, $R_9 = R_3 = 1$ kΩ, $R_4 = 50$ kΩ, $R_{10} = 3.3$ kΩ are calculated from Eqs. (15) and (16). According to the feedback control system structure as well as the system equations, and then further adjusting the resistance values of resistors R_1, R_7, R_8, R_9, R_{13} on the chaotic circuit, the hardware circuit of the memristor stochastic resonance system can be obtained, as shown in Fig. 13. In this stochastic resonance system circuit, the signal to be detected is first inputted through the reverse input port of the inverter U5, and subsequently accessed by the output port of the inverter to the y-dimensional circuit portion, while the y-dimensional output can be treated as an output signal, namely, the signal output from the output port of U30.

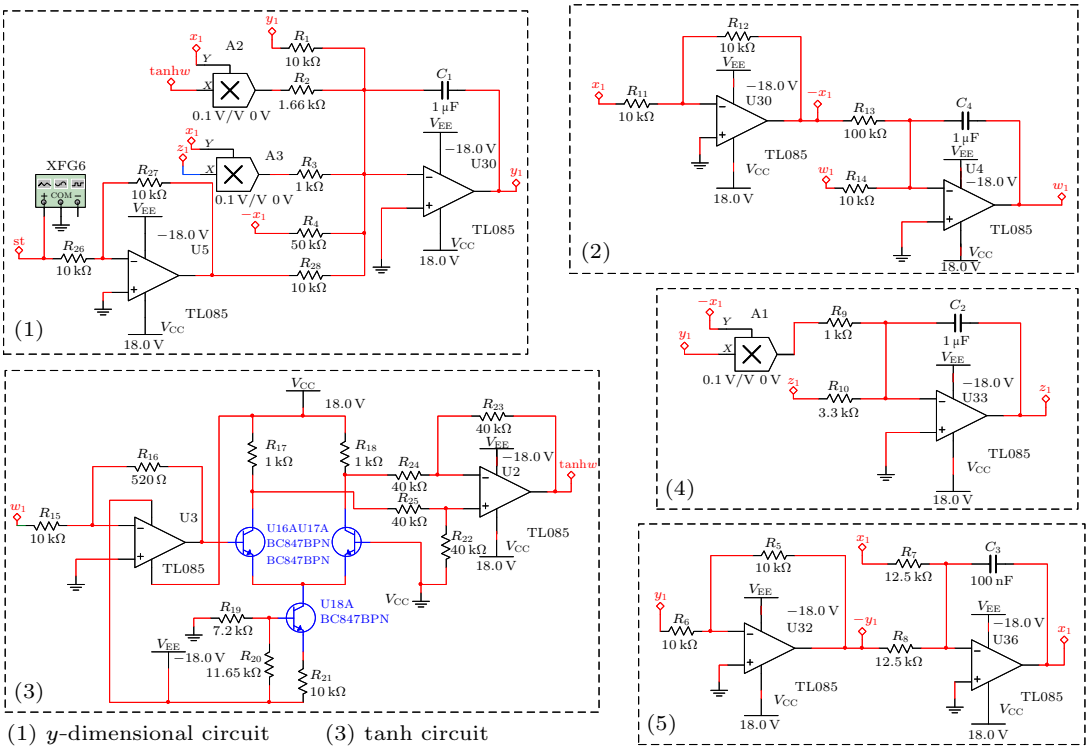


Fig. 13. Memristor stochastic resonance circuit.

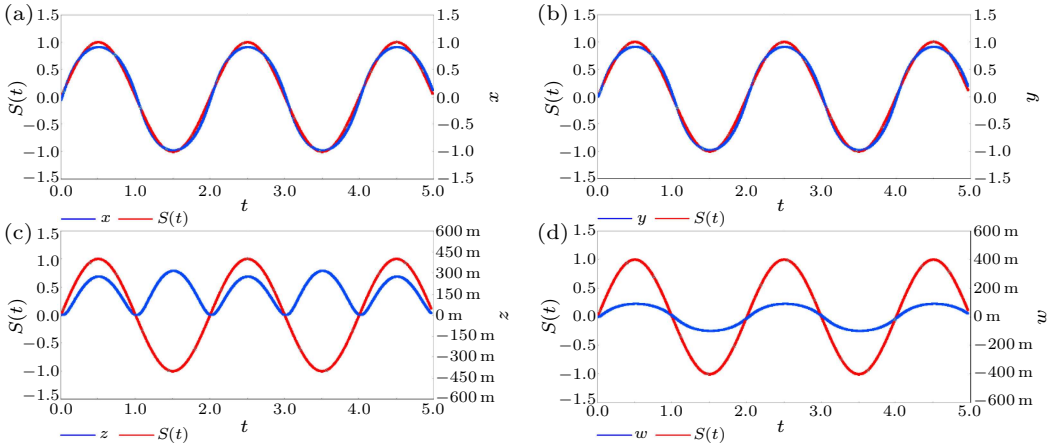


Fig. 14. Memristor stochastic resonance circuit output waveform and input waveform $S(t)$: (a) x-dimensional output signal; (b) y-dimensional output signal; (c) z-dimensional output signal; (d) w-dimensional output signal.

In this paper, we also set the input signal $S(t)$ to a noise-free condition and the amplitude $A = 1$, the performance evaluation of this circuit is simulated and analyzed and the Multisim simulation results are clearly shown in Fig. 14. In this result graph, the input signal $S(t)$ is marked with red lines, while the blue lines represent the output signals of the circuit after processing in each dimension. It can be observed from Fig. 14, in which the x and y dimensions have been reduced to a certain extent to the original signal, which basically restores the characteristic signal, that the z and w dimensions are less desirable, and the characteristics of this output signal coincide with the expected results deduced based on the circuit theory, and also maintain a high degree of consistency with the results obtained from Fig. 9(a). Similarly, the x-dimensional output signal, as shown in Fig. 11(a), remains highly consistent with the y-dimensional output signal, as shown in Fig. 11(b), under the input signal without noise. This comparison result not only verifies the correctness of the circuit design, but also further confirms the validity and accuracy of the simulation model.

4. Conclusion

In this paper, in the process of exploration of the nonlinear dynamical properties of memristor, the memristor stochastic resonance phenomenon is successfully induced by using memristor chaos. The main work of this paper is as follows: through the dynamic analysis of the phenomenon, it is revealed that the memristor chaotic system can interact nonlinearly with the external environmental noise under the change of certain parameters, which in turn generates the phenomenon of memristor stochastic resonance. In addition, the equilibrium analysis is carried out, which reveals that its essence is a single potential well stochastic resonance. Second, in the gain analysis of the constructed system together with theoretical modelling simulation, the following is found: the constructed system can be denoised for noise-containing signals, and for input signals within a certain amplitude range, the characteristic signals can be amplified. Finally, the practicality and reliability of the constructed model are further verified by circuit simulation, which provides strong support for the practical application of the stochastic resonance model based on memristor chaos.

References

[1] Tian H, Zhao M, Liu J, Wang Q, Yu X and Wang Z 2024 *Fractal Fractional* **8** 307
[2] Li H, Yang Y, Li W, He S and Li C 2020 *Eur. Phys. J. Plus* **135** 80
[3] Xu B, Wang G, Iu H H, Yu S and Yuan F 2019 *Nonlinear Dynam.* **96** 765
[4] Shamsher U, Jiangbin Z, Nizamud D, Tanveer H M, Farhan U and Mahwish Y 2023 *Comput. Sci. Rev.* **47** 100530
[5] Ramesh R, Karthikeyan R, Dolvis G L, Ondrej K, Hamidreza N and Iqtadar H 2022 *Chaos Soliton. Fract.* **156** 111834
[6] Li C, Min F H and Li C B 2018 *Nonlinear Dynam.* **94** 2785
[7] Jia S H, Li Y X, Shi Q Y and Huang X 2022 *Chin. Phys. B* **31** 070505
[8] Zhang F F, Huang Z, Kou L, Li Y and Cao M Y 2023 *Chin. Phys. B* **32** 010502
[9] Wang S M, Peng Q Q and Du B X 2022 *Opt. Laser Technol.* **148** 107753
[10] Yu J, Zeng F, Wan Q, Lu Z and Pan F 2023 *InfoMat* **5** e12458
[11] Suo J, Wang H Y, Yan Y S and Shen X H 2024 *Nonlinear Dynam.* **113** 5193
[12] Cui T H, Li J, Yuan Q, Wei Y Q, Dai S Q, Li P D, Zhou F, Zhang J Q, Chen L and Feng M 2023 *Chin. Phys. Lett.* **40** 080501
[13] Jiao S, Hou T, Jiao T Y, Wang Y and Song N L 2024 *Chin. J. Phys.* **91** 220
[14] Wang X, Xiong X, Li C, Wu B and Niu L 2024 *Chin. J. Phys.* **91** 11
[15] Dai F, Chen J, Liu C, Chen Z and Peng D 2024 *Measurement* **237** 115183
[16] López C, Naranjo á, Lu S and Moore K J 2022 *J. Sound Vib.* **528** 116890
[17] Jiang Z, Zhang G and Gao Y 2025 *Appl. Math. Model.* **137** 115657
[18] Zhou Z B and Yu W X 2022 *Int. J. Bifurcat. Chaos* **32** 2250154
[19] Chua L 2015 *Radioengineering* **24** 319
[20] Sun S Z, Li J P and Li X Y 2023 *J. Lanzhou University* (Natural Sciences) **59** 387